Journal of Applied Electrochemistry (2006) 36:1333–1339
DOI 10.1007/s10800-006-9167-2

A low external temperature method for synthesis of active electrode materials for Li batteries – Part B: Synthesis of lithium iron oxides $Li_xFe_yO_z$

S. UZUNOVA[1,*], I. UZUNOV[2], D. KOVACHEVA[2], A. MOMCHILOV[1] and B. PURESHEVA[1]
[1]*Institute of Electrochemistry and Energy Systems (former CLEPS), Bulgarian Academy of Sciences, Acad. G.Bonchev Str., bl.10, 1113, Sofia, Bulgaria*
[2]*Institute of General and Inorganic Chemistry, Bulgarian Academy of Sciences, 1113, Sofia, Bulgaria*
*(*author for correspondence, e-mail: uzunov_iv@igic.bas.bg)*

Received 28 June 2005; accepted in revised form 5 June 2006

Key words: fluidized bed, lithium batteries, lithium ferrite, low temperature synthesis, solid state reaction

Abstract

Anode materials for lithium-ion batteries based on iron oxides were synthesized using two different methods: a Low External Temperature Method (LETM) and a conventional Solid State Reaction Method (SSRM). Both methods lead to the formation of final products representing a mixture of two phases: approximately 75% $LiFeO_2$ and 25% $Li_{-x}Fe_5O_8$ ($0 < x \leq 0.1$). When compared with the ordinary solid state synthesis, LETM creates conditions for carrying out the synthesis at a lower external calcination temperature (200 °C) over a shorter period. The properties of the $Li_xFe_yO_z$ obtained by the LETM were compared with those of the same compound obtained by SSR at 700 °C. Higher initial discharge capacity was displayed by the sample synthesized by the SSR method, while a superior cycling stability was shown by the sample synthesized by the LETM. The latter shows approximately double capacity at the 30th cycle as compared with the sample synthesized by SSRM.

1. Introduction

A large number of substances have been studied for use as active materials in lithium batteries with high energy density and good cycling life. Many research groups have investigated various cathode materials such as a layered oxides with general formula $LiMO_2$ (M = Co, Ni, Mn, Fe), which are built of alternating layers of trigonally distorted MO_6 and LiO_6 edge sharing octahedra [1–3]. Recently, iron-based compounds have attracted attention as active materials for rechargeable Li batteries [4–6].

Lithium ferrite, $LiFeO_2$, has important advantages compared to $LiCoO_2$ and $LiNiO_2$ for practical use, because it is non-toxic and contains the most abundant and low cost metal available. It is known that $LiFeO_2$ crystallizes in three polymorphic modifications (α, β or γ) depending on the synthesis and processing procedures. α-$LiFeO_2$ has a cubic disordered rock salt structure while γ-$LiFeO_2$ has a tetragonal structure in which the Li^+ and Fe^{3+} ions order along the tetragonal c axis. β-$LiFeO_2$ appears to be an intermediate phase formed during the ordering process. Unfortunately, none of these three modifications shows promising cathode properties in rechargeable lithium cells [7–10]. As a result, attention has been focused on the synthesis of metastable forms of $LiFeO_2$ by soft chemistry processes.

A review of the studies on mixed lithium iron oxides has revealed that almost all of them were obtained through complex reaction mechanisms (e.g. ion exchange reaction, hydrothermal method and etc.).

Recently, two kinds of $LiFeO_2$ materials have been reported, orthorombic $LiFeO_2$ obtained at low temperature (150 °C) and $Li_xFe_yO_z$ obtained at high temperature (800 °C) [11, 12]. Furthermore, Kanno et al. also reported a new type of $LiFeO_2$ material with a tunnel structure, which showed fairly good lithium insertion/extraction within the voltage range of 1.5–4.5 V [13]. However, many problems still remain such as a low operating voltage (2 V), poor electrochemical activity, especially for the cubic α and γ-forms and low capacity retention during the cycling tests.

Despite the poor electrochemical characteristics as a cathode in lithium-ion batteries, $LiFeO_2$ has been investigated as an anode material within the voltage range 0.01–2.5 V vs. Li/Li^+. In this case the material displays an average discharge voltage of 1 V, which renders it very promising for use as active material for the negative electrode in lithium-ion rechargeable batteries. It has been shown that the mechanism of lithium reactivity with $LiFeO_2$ within the 0.01–2.5 V range differs from the classical Li intercalation or Li alloying process and involves the formation and decomposition of Li_2O accompanying the reduction and oxidation of metal nanoparticles, respectively [14].

A summary of literature data has shown that synthesis conditions of lithium–iron oxides strongly affect their electrochemical properties [15–17].

In this paper we compare the electrochemical characteristics of $Li_xFe_yO_z$ synthesized by a Low External Temperature Method (LETM) and by a conventional solid state reaction (SSRM) as a cathode (within the voltage range 1.5–4.3 V vs. Li/Li^+) and anode (within the voltage range 0.01– 2.5 V vs. Li/Li^+) active material [18]. Our investigations are aimed at the synthesis of $Li_xFe_yO_z$ at a ratio Fe:Li = 2:1 since no data exist for the electrochemical behaviour of this compound.

2. Experimental

Mixed lithium-iron oxides $Li_xFe_yO_z$ were synthesized by the LETM method and SSRM using $Fe(NO_3)_3 \cdot 9H_2O$ and $LiNO_3$.

In the case of the LETM initial compounds were dissolved in distilled water. Appropriate volumes of these solution were mixed in order to obtain an Fe:Li ratio of 2:1. The precursor (Pr1) was prepared by drying droplets of the mixed solution in a liquid drying agent (transformer oil – IEC 60 296) heated to 180 °C. To remove the transformer oil, the precursor was rinsed with petroleum ether until a colourless eluent was obtained. Nevertheless, a residual amount of oil remains trapped in the particle pores. The precursor was calcinated at 200 °C in a fluidized bed reactor for 4 h.

A mixture of the two components (Pr2) was calcinated at different temperatures (200, 300, 400 and 700 °C) in a furnace over 24 h, with the material periodically crushed (SSRM).

X-ray analysis was carried out using a Philips ADP15 diffractometer with CuK_α radiation in order to identify the crystalline phases present in the synthesized powders. Diffraction data were processed with the Powder Cell program to determine the approximate stoichiometry of synthesized phases [19].

Thermal analysis (DTA and DTG) was performed with a DERIVATOGRAPH-1500 combined thermal analyzer, in a platinum crucible, in air, at a heating rate of 10 °C min^{-1}.

The electron micrographs were obtained using a JEOL-Superprobe 733.

The electrochemical behavior of synthesized materials was investigated in a three-electrode cell with a Li/Li^+ reference electrode using computer controlled laboratory cycling equipment. The negative electrode was lithium foil. The positive electrode composites were prepared from the active material (15 mg ± 2) with Teflonized Acetylene Black (TAB-2) at a 1:1 weght ratio. The obtained mass was pressed onto Cu-foils and Al-foils (15 mm diameter) at a pressure of 10 t cm^{-2}. The used electrolyte was a mixture of 1 M $LiClO_4$ ethylene carbonate/dimethyl carbonate (EC/DMC 1:1 ratio). The water content in the electrolyte was less than 30 ppm. All assemblies were carried out in an argon-filled dry box. The cells were cycled at room temperature within the voltage range 0.01–2.5 V (copper foils) and 1.5–4.3 V (aluminium foils) vs. Li/Li^+. The current density was 0.57 mA cm^{-2}.

3. Results and discussion

3.1. *Thermal analysis (DTA/DTG)*

The DTA/DTG curves of the initial compounds $Fe(NO_3)_3 \cdot 9H_2O$ and $LiNO_3$ are shown in Figure 1a and b. Iron nitrate decomposes into Fe_2O_3 during heating within the temperature range 100–200 °C, denoted by clear endothermic effects at 124, 134 and 180 °C displayed by the DTA curve. The $LiNO_3$ DTA curve is characterized by a broad endothermic effect within the 500–750 °C range, related to its decomposition.

The DTA/DTG curves of Pr1 and Pr2 are shown in Figure 1c and d. The DTA curve of Pr1 shows a broad triple exothermic effect within the range 200–400 °C characterized by maxima at a 260, 320 and 370 °C and a slight endothermic effect with a maximum at 552 °C. The first effect is attributable to the solid state reaction of the initial components, as well as the burning of transformer oil residues in the precursor. The endothermic effect is connected with the decomposition of residual amounts of $LiNO_3$.

The DTA/DTG curves of the mechanical mixture of $LiNO_3$ and $Fe(NO_3)_3$, (Pr2), illustrate the decomposition of the initial compounds within the ranges 370–520 °C for lithium nitrate and 100–250 °C for iron nitrate. No evidence for the type of solid state reaction seen in the case of Pr1 was observed.

These results show that the synthesis of $Li_xFe_yO_z$ system from Pr1 occurs within the temperature range 200–400 °C as a self-combustion reaction, due to the presence of an organic phase which burns with a calorific effect of 48 MJ kg^{-1} (LETM).

3.2. *X- ray analysis*

The structural changes during the heating of Pr1 and Pr2 under fluidized bed conditions and SSR were investigated by X- ray analysis.

The X-ray patterns of Pr1 (200 °C), Figure 2a, show the presence of α-Fe_2O_3 and an amount of unreacted $LiNO_3$. These results suggest that the formation of Pr1 is related to a partial decomposition of the initial components. Diffraction lines of two phases, approximately 75% α-$LiFeO_2$ and 25% $Li_{1-x}Fe_5O_8$ ($0 < x \leq 0.1$) are observed during the calcination of Pr1 under fluidized bed conditions for 4 h at 200 °C, (called sample S1).

The X-ray patterns of Pr2 contain the diffraction lines of the initial components – lithium and iron nitrates, Figure 2b. During the calcination of Pr2 at 200 °C diffraction lines of $LiNO_3$, which has not undergone

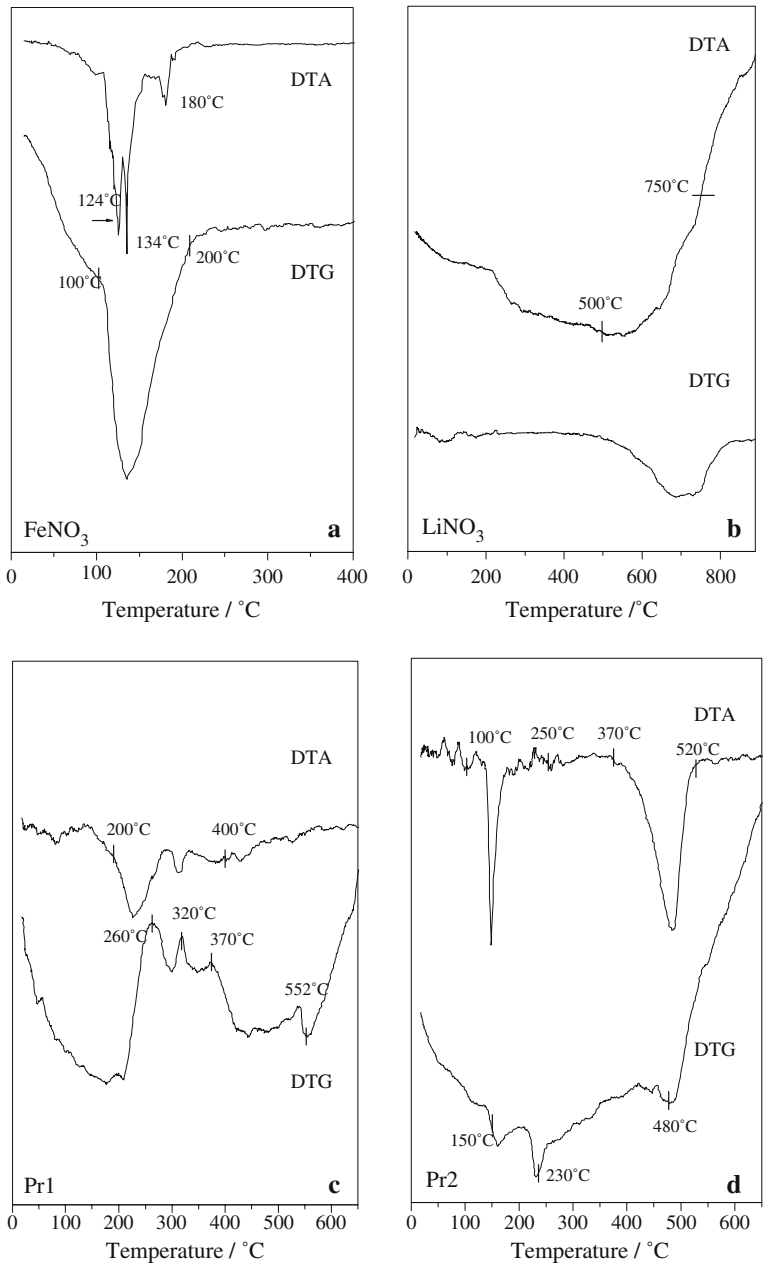

Fig. 1. Thermal analysis (DTA/DTG) of (a) iron nitrate, $Fe(NO_3)_3 \cdot 9H_2O$; (b) lithium nitrate, $LiNO_3$; (c) precursor, Pr1 and (d) precursor, Pr2.

decomposition and α-Fe_2O_3 (hematite) are observed, indicating the decomposition of $Fe(NO_3)_3$. The phase composition remains unchanged when the temperature is increased from 200 to 300 °C, but the half width of the diffraction peaks decreases as a result of increased crystallite size.

During the calcination of the Pr2 sample at 400 °C, in addition to the diffraction lines of α-Fe_2O_3 (h) and β-$LiFeO_2$ (75%), a residual amount of non-decomposed $LiNO_3$ is observed. At 700 °C only diffraction lines of the two phases – approx. 75 % α-$LiFeO_2$ and 25% $Li_{1-x}Fe_5O_8$, ($0 < x \leq 0.1$) are observed, (called sample S2). Therefore it can be accepted that for the SSR method the final product is formed only when 700 °C is reached. The phase transformations during the thermal treatment of Pr1 and Pr2 under LETM and SSR conditions are shown in Figure 3.

The X-ray analysis data of $Li_xFe_yO_z$ synthesized using identical components under different conditions provide evidence that both methods lead to the formation of similar final products, i.e. identical mixture of two phases: approx. 75% α-$LiFeO_2$ and 25% $Li_{1-x}Fe_5O_8$, which corresponds to the formula $Li_{1-0.25x}Fe_2O_{3.5}$, $0 < x \leq 0.1$.

Comparing the conventional solid state synthesis with the LETM, the latter offers possibilities to ensure high reaction rate at a relatively low external calcination temperature of 200 °C. The same products are formed by the conventional solid state reaction method and are only obtained at a temperature of 700 °C.

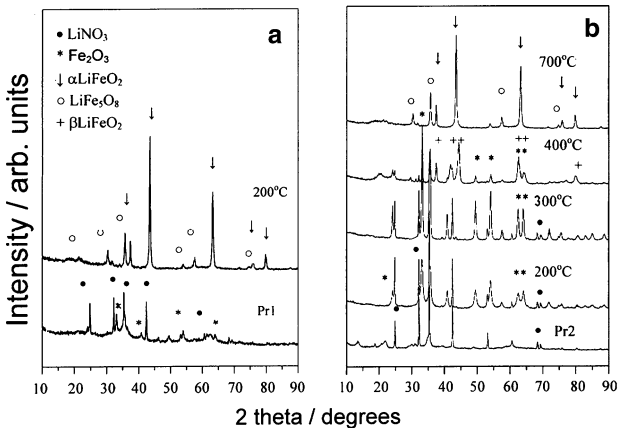

Fig. 2. X-ray diffraction patterns of $Li_xFe_yO_z$ synthesized by (a) LETM method and (b) solid state reaction.

3.3. *SEM investigations of the $Li_xFe_yO_z$ morphology*

The particle sizes of materials synthesized by both methods was determined by SEM investigations. The micrographs are presented in Figure 4a and b. It was established that the particle sizes of sample S1 vary within the range 50–100 nm, while S2 sample shows grain sizes 500–600 nm. A similar difference in the particle size of the two products is due to the effect of calcination temperature and synthesis conditions [20–22]. The synthesis of sample S1 proceeds as a self-combustion reaction with the mutual isolation of the particles under fluidized bed conditions thus ensuring a final product with smaller particle size.

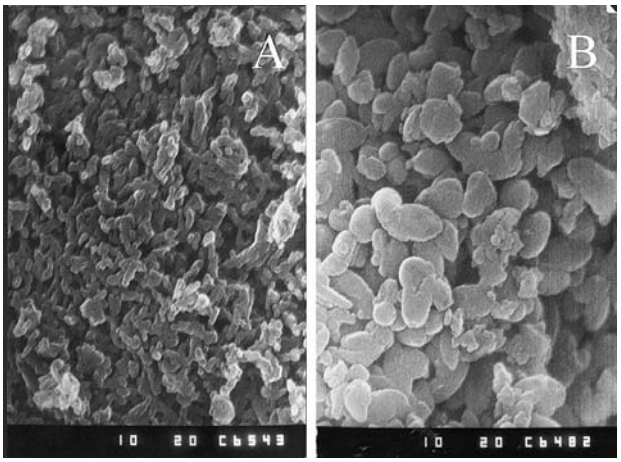

Fig. 4. SEM micrographs of $Li_xFe_yO_z$ synthesized by (a) LETM at 200 °C and (b) SSRM at 700 ° C.

3.4. *Electrochemical characteristics of $Li_xFe_yO_z$*

3.4.1. *Electrochemical characteristics of $Li_xFe_yO_z$ within the voltage range 1.5–4.3 V*

The charge and discharge behaviour between 1.5 and 4.3 V of Li/S1 and Li/S2 cells and a current density 0.57 mA cm^{-2} is depicted in Figure 5. It is clear that the electrochemical lithium deintercalation reaction is hindered and only 0.096 atoms Li for S1 and 0.31 atoms Li for S2, per mole $LiFe_2O_{3.5}$ can be extracted, which corresponds to capacities of 27 mAh g^{-1} (S1) and 87 mAh g^{-1} (S2). The superior electrochemical behaviour of sample S2 can be explained by the higher

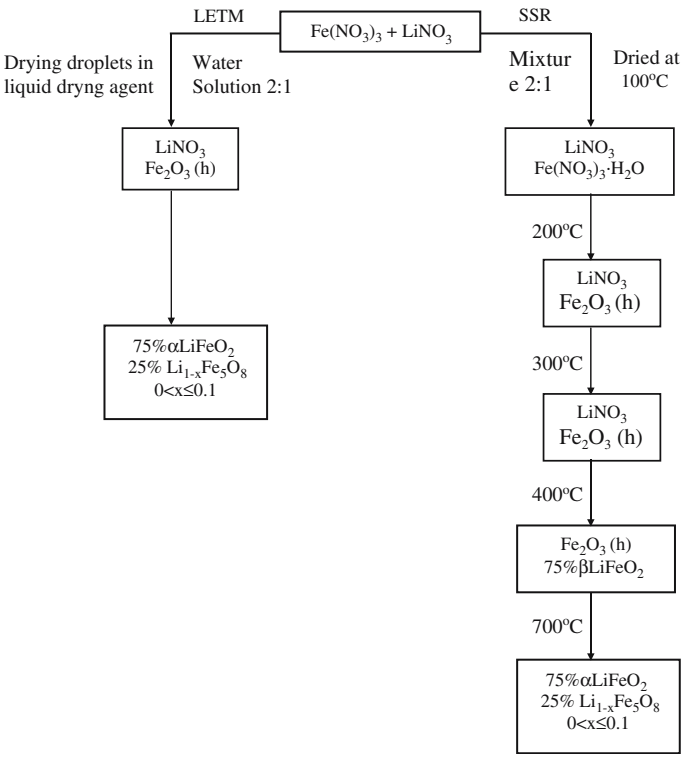

Fig. 3. Diagram of the phase transformations during the thermal treatment of Pr1 (LETM) and Pr2 (SSRM).

crystallinity. After the first charge at 4.3 V no plateaus were observed in both cycling curves.

These results provide evidence that the use of $Li_xFe_yO_z$ synthesized by the proposed methods as a cathode material for lithium-ion batteries is limited.

3.4.2. *Electrochemical characteristics of $Li_xFe_yO_z$ within the voltage range 0.01–2.5 V*

The first two discharge and the first charge curves of a Li | 1 M $LiClO_4$ EC/DMC |$Li_xFe_yO_z$ cells with two materials S1 and S2 and a current density of 0.57 mA cm^{-2} are shown in Figure 6. For both samples at the first discharge process, the potential drops rapidly to a plateau at 0.75 ± 0.1 V and then continuously decreases to a cut-off voltage of 0.01 V. All discharge curves show high Li content at the end of the discharge from 8.9 to 10.6 Li atoms per mole $LiFe_2O_{3.5}$, corresponding to 1500 mAh g^{-1} for S1 and 1800 mAh g^{-1} for S2.

This can be explained by a defectless structure and higher crystallinity of sample S2, leading to improvement in the electrochemical behaviour of the material during initial lithiation [21].

For the electrochemical reaction of $LiFe_2O_{3.5}$ with lithium:

$$LiFe_2O_{3.5} + 6Li \rightarrow 2Fe + 3.5Li_2O \quad (1)$$

where 6 e^- shift from Li^o to $LiFe_2O_{3.5}$; the theoretical capacity (Q_t) is 920 mAh g^{-1}.

The observed substantial surplus capacity, approximately 600 mAh g^{-1}, can be explained by the participation of TAB in the electrochemical reaction.

During the following charge the cells display capacities within the range 660–920 mAh g^{-1} and gradual increase of voltage within the range 1.8 ± 0.3 V. The very large hysteresis of the reduction and oxidation potentials (about 0.8 V) seems to be related to crystal chemical changes that occur, due to the reduction associated with Li insertion.The second and the next discharge curves differ considerably from the first, suggesting drastic, lithium driven, structural or textural modifications showing that the mechanism of the electrochemical reaction is not the same as during the initial lithiation. A clear-cut plateau is observed at 1.0 V.

Further cycling proceeds in a reversible three-phase region between the metal oxide, the reduced metal and lithium, according to the reaction [14]:

$$yLi_2O + Fe \leftrightarrow Li_\alpha Fe_yO_\beta + (y-\beta)Li_2O + (2\beta-\alpha)Li \quad (2)$$

The reversible capacity of the first cycle for S1 is 900 mAh g^{-1}, while for S2 it is 580 mAh g^{-1}.

The electrochemical behaviour of Li/S1 and Li/S2 cells during cycling is presented in Figure 7. It should be noted that two samples show considerable capacity loss during the first cycle: for S1 – 600 mAh g^{-1} and for S2 – 1220 mAh g^{-1}. After the second and following cycles

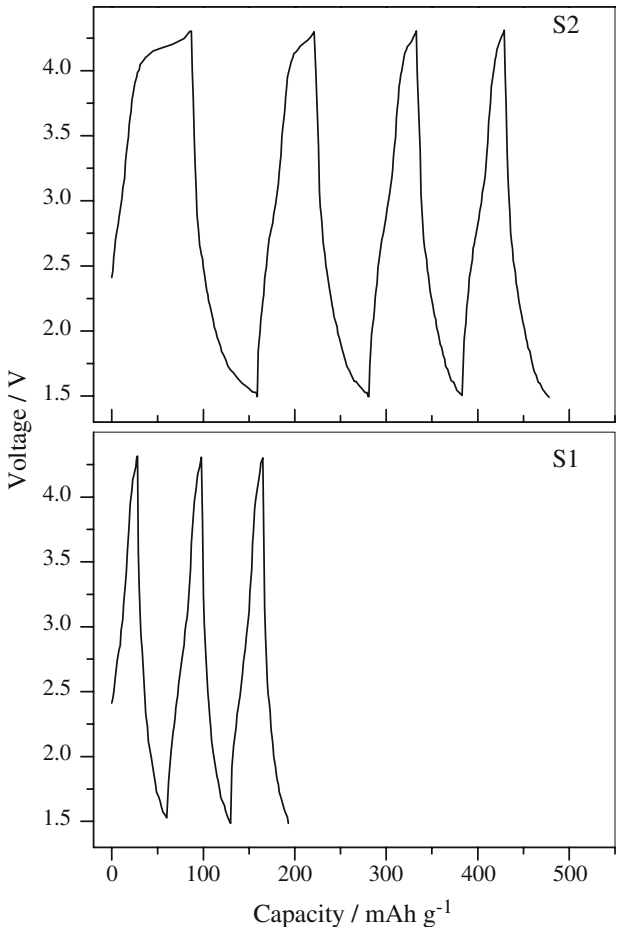

Fig. 5. Charge–discharge curves of Li/S1 and Li/S2 cells within the voltage range 1.5–4.3 V.

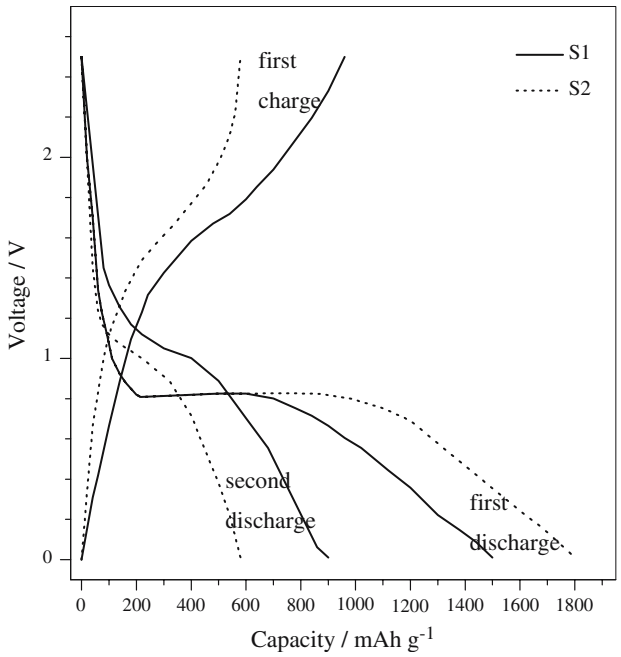

Fig. 6. Voltage vs. capacity of sample S1 (LETM) and sample S2 (SSRM) for the first two lithiations and the first delithiation of Li/S1 and Li/S2 cells within the voltage range 0.01–2.5 V.

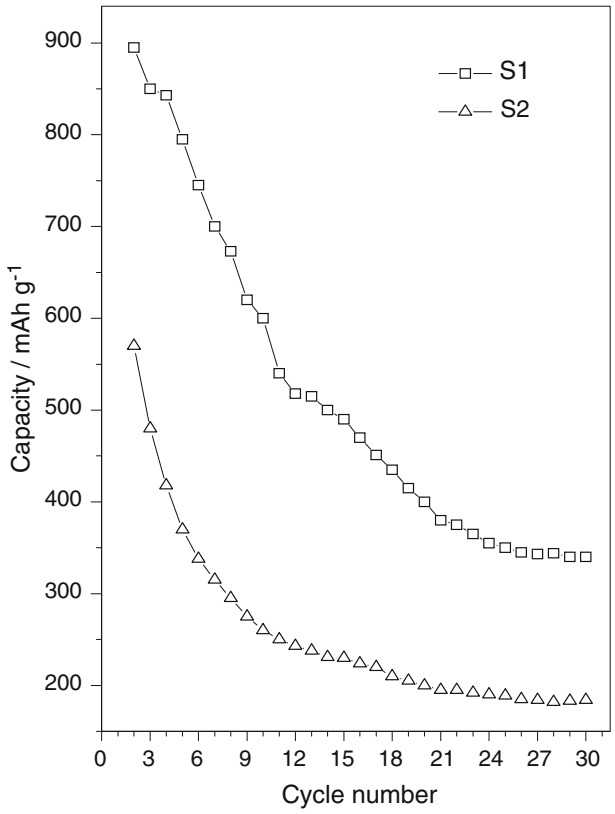

Fig. 7 Long term cycling behaviour of sample S1 (LETM) and sample S2 (SSRM).

the losses decrease substantially up to 10th cycle – 38 mAh g^{-1} and up to 30th cycle – 18 mAh g^{-1}.

At the 30th cycle sample S1 shows approximately double the capacity as compared to S2. The reason for this phenomenon is the fact that capacity losses depend exclusively on the extent of fragmentation of the particles during the first discharge. During this fragmentation the crystal phase is transformed into an amorphous material with particle size smaller than 5 nm. These drastic structural alterations lead to the loss of contact between the individual particles on one hand and between the particles and the conductive matrix of TAB on the other hand, hence leading to capacity loss during cycling.

Sample S1 was composed of numerous small nano-sized particles (Figure 4a and b) and these nano-particles improved the structural stability of S1 powder, even though this affected the structural changes in the first cycle. This leads to smaller capacity losess during continuous cycling of the Li/S1 cell. The particles size of sample S2 is five to six times larger than in the case of S1. The particles are subject to drastic changes during initial lithiation, hence leading to capacity loss during the lithiation of Li/S2 cell.

4. Conclusions

Lithium–iron oxides were synthesized applying a low external temperature method (LETM) and a conventional solid state reaction method (SSRM). Both methods lead to the formation of final products representing a two-phase mixture – approximately 75% $LiFeO_2$ and 25 % $Li_{1-x}Fe_5O_8$, where ($0 < x \leq 0.1$). The LETM is suitable for the preparation of mixed lithium iron oxides which, when synthesized using conventional solid state reaction methods at high temperatures, yields final products with larger particle sizes. The LETM provides conditions for carrying out the synthesis at a lower external calcination temperature (200 °C) over a shorter period.

Using different preparation methods, synthesis temperatures and oxygen access during calcination, we have the possibility to determine how the electrochemical behaviour of $Li_xFe_yO_z$ is affected.

The material synthesized by LETM is a potential candidate as active material in negative electrodes of lithium batteries. Higher initial discharge capacity was displayed by the sample synthesized by the classical solid state method, while a superior cycling stability was shown by the sample synthesized by the LETM (340 mAh g^{-1} at 30th cycle).

The advantage of the mixed lithium iron oxide materials synthesized through LETM as compared to the carbonaceous anode materials is the reversible capacity which is about twice that of graphite (372 mAh g^{-1}) and allows for good cycling at room temperature.

Acknowledgment

The authors gratefully acknowledge financial support by The Bulgarian Science Foundation: Contract X – 1412.

References

1. J.K. Dahn, U. Von Sacken and C.A. Michel, *Solid State Ionics* **44** (1990) 87.
2. H. Arai, S. Okada, Y. Sakurai and J. Yamaki, *Solid State Ionics* **95** (1997) 275.
3. Y.I. Jang, B. Huang, H. Wang, D.K. Sadoway and Y.M. Chiang, *J. Electrochem. Soc.* **146** (1999) 3217.
4. S.-K. Chang, H.-J. Kim and S.-T. Hong, *J. Power Sources* **119** (2003) 69–75.
5. R. Kanno, T. Shirane, Y. Kawamoto, Y. Takeda, M. Takano, M. Ohashi and Y. Yamaguchi, *J. Electrochem. Soc.* **143**(8) (1996) 2435.
6. K. Padhi, K.S. Nanjundaswamy, C. Masquelier, S. Okada and J.B. Goodenough, *J. Electrochem. Soc.* **144** (1997) 1609.
7. J.C. Anderson and M. Schiebor, *J. Phys. Chem. Solids* **25** (1964) 961.
8. K. Kanno, T. Shirane, Y. Kawamoto, Y. Takeda, M. Takano, M. Ohashi and Y. Yamaguchi, *J. Electrochem. Soc.* **146** (1996) 2435.
9. K. Ado, M. Tabuchi, H. Kobayashi, H. Kageyama, O. Nakamura, Y. Inaba, K. Kanno, M. Takagi and Y. Takeda, *J. Electrochem. Soc.* **144** (1997) L177.
10. Y. Sakurai, H. Arai and J. Yamaki, *Solid State Ionics* **29** (1998) 113.

11. Y.S. Lee, C.S. Yoon, Y.K. Sun, K. Kobayakawa and Y. Sato, *Electrochem. Commun.* **4** (2002) 727.
12. Y.S. Lee, S. Sato, M. Tabuchi, C.S. Yoon, Y.K. Sun, K. Kobayakawa and Y. Sato, *Electrochem. Commun.* **5** (2003) 549.
13. T. Matsumura, K. Kanno, Y. Inaba, Y. Kawamoto and M. Takano, *J. Electrochem. Soc.* **149** (2002) L1509.
14. M.N. Obrovac, K.A. Dunlap, K.J. Sanderson and J.K. Dahn, *J. Electrochem. Soc.* **148**(6) (2001) 576.
15. P. Poizot, S. Laruell, S. Grugeon, L. Dupont and J.-M. Tarascon, *Nature* **407** (2002) 496.
16. S. Morzilli, B. Scorosati and F. Sgarlata, *Electrochim. Acta* **30**(10) (1985) 1271.
17. X. Wu and S.-B. Kim, *Electrochem. Solid-State Lett.* **2**(4) (1999) 184.
18. S. Uzunova, B. Banov, A. Momchilov, S. Vassilev, T. Stankulov and I. Uzunov, *J. Appl. Electrochem.* **35** (2005) 117.
19. W. Kraus and G. Nozle, *Powder Cell Program for Windows, version 2.4* (BAM, Berlin, 2002).
20. K.T. Hwang, W.S. Um, H.S. Lee, J.K. Song and K.W. Chung, *J. Power Sources* **74** (1998) 169.
21. Y. Li, C. Wan, Y. Wu, C. Jiang and Y. Zhu, *J. Power Sources* **85** (2000) 294.
22. T. Tsumura, A. Shimizu and M. Inagaki, *J. Mater. Chem.* **14** (1993) 995.